Effects of High Strain Rates on ASTM A992 and A572 Grade 50 Steel

Matthew P. Murray; U.S. Army Engineer Research and Development Center; Vicksburg, Mississippi, USA

Stephen P. Rowell; U.S. Army Engineer Research and Development Center; Vicksburg, Mississippi, USA

Trace A. Thornton; U.S. Army Engineer Research and Development Center, Vicksburg, Mississippi, USA

ABSTRACT

Uniaxial tension tests were conducted on ASTM A572-50 and A992 steel at increasing strain rates to determine material strength properties of structural members subjected to dynamic loadings. The increase in dynamic yield strength and ultimate tensile strength, defined as the dynamic increase factor (DIF), versus strain rate was determined to provide the necessary information to efficiently design blast resistant structures utilizing modern day structural steel. Dynamic strength properties were determined by high-rate tensile tests using a hydraulic testing apparatus and compared to static values obtained from ASTM E8 standard tension tests. The comparisons were used to calculate the DIF of each steel at strain rates ranging from 0.002 to 2.0 inch/inch/second. Experiments revealed that A572-50 steel exhibited an increase in yield strength up to 35% and ultimate tensile strength up to 20% as strain rate increased over the range tested. A992 steel exhibited a similar increase in yield strength up to 45% and ultimate tensile strength up to 20%. DIF versus strain rate curves obtained during this research will be used to develop criteria within the structural steel design chapter of Unified Facilities Criteria (UFC) 3-340-02 (2014) for A572-50 and A992 steel.

INTRODUCTION

Understanding the change in material properties with change in loading rates has been addressed by many researchers over the past century and is vital to accurate design and evaluation of structural members subjected to blast loads [1–10]. The ratio of dynamic yield strength to static is defined as the dynamic increase factor for yield (DIF_y) and is known to be a function of strain rate [11–18]. Similarly, the ratio of dynamic to static ultimate tensile strength (UTS) is defined as the dynamic increase factor for UTS (DIF_u). Specification of the DIF of a material provides engineers with the capability to efficiently design structural members to resist large loads produced during dynamic blast phenomena [19–21]. DIF design curves for different materials are empirically derived from experimental material property tests conducted at increasing strain rates.

Engineers and scientists throughout the protective design community have recognized cost and performance benefits of incorporating newer, readily available, advanced construction materials into hardened structure designs for protection of personnel, critical assets, and facilities. The reinforced concrete design chapter of UFC 3-340-02, *Structures to Resist the Effects of Accidental Explosions* [19], uses DIF design curves developed by Malvar and Crawford [22,23] for different grades of ASTM A615 reinforcing steel. The structural steel design chapter of the UFC currently provides DIF design curves for ASTM A36 and A514 structural steel [19]. However, there is limited design guidance available in the current UFC to permit efficient use of more modern steels, specifically A572-50 and A992, due to the lack of research on these steels under high strain rates.

The U.S. Army Engineer Research and Development Center (ERDC) was tasked by the Department of Defense Explosives Safety Board (DDESB) to conduct a series of static and dynamic, uniaxial tension tests on A572-50 and A992 steel. The material strength data were used to develop DIF_y and DIF_u versus strain rate curves for these steels. The experimental curves will later be used to develop design DIF curves for incorporation into future revisions of the structural steel design chapter in the UFC.

PROCEDURE

Test Specimen

ASTM A572-50 [24] specimens were fabricated from a domestic, nominal 0.375-in.-thick plate. The mill test report (MTR) indicated that the plate also met the specifications of ASTM A709-50 [25]. ASTM A992 [26] specimens were obtained from the web of domestic S12x31.8 beams, which had a nominal thickness of 0.35 in. The MTR for the A992 steel indicated the beam also met specifications of ASTM A6 [27], A709-50 [25], A572-50 [24], and A36 [28]. The chemical composition of the tested materials is listed in Table 1, as specified by the MTRs.

Table 1. Chemical composition of tested materials (weight percent).

Material	C	Mn	P	S	Si	Al	Cu	Ni	Cr	Mo	Cb/Nb	V	Ti
A572-50 Plate	0.17	1.04	0.009	0.002	0.19	0.027	0.22	0.19	0.12	0.07	0.001	0.042	0.002
A992 Beam	0.07	1.21	0.01	0.022	0.2	0.001	0.28	0.1	0.1	0.048	0.001	0.031	-

Static-rate specimen were waterjet cut to ASTM E8 [29] standard sheet-type geometries. Dynamic-rate specimens were waterjet cut into a modified pin-type specimen geometry shown in Figure 1 with tolerances similar to those in ASTM E8. The full thickness of the parent material was used. Bolt holes were drilled using a computer numerical control (CNC) machine. Figure 2 provides a visual comparison of the static and dynamic specimens.
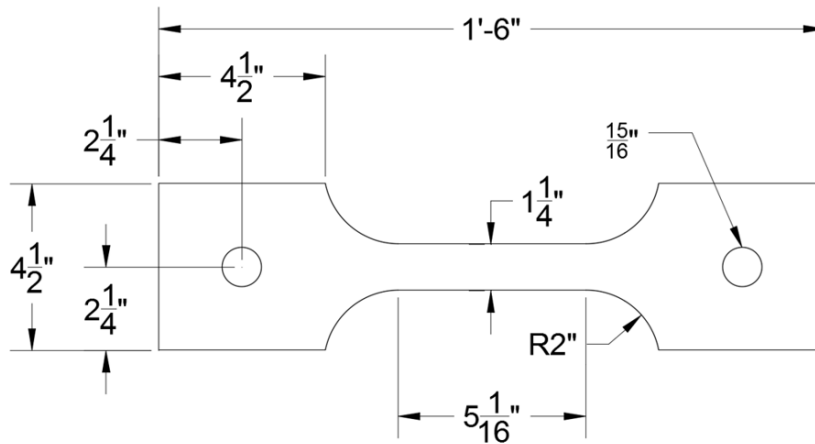

Figure 1. Dynamic uniaxial tension specimen geometry.

Figure 2. Static (top) and dynamic (bottom) uniaxial tension specimens.

Equipment

Static Tension Test Apparatus

ERDC's Instron 33R4206 Universal Testing System (Figure 3) was used to conduct the static, uniaxial tension tests. An integrated optical extensometer was used to record elongation over time. The apparatus allowed controlled-rate testing at an average elastic strain rate of approximately 0.00002 s^{-1}.

Figure 3. Instron uniaxial tension test machine used for static-rate testing.

Dynamic Tension Test Apparatus

ERDC's 200-kip-capacity hydraulic loader (Figure 4) was used to conduct the dynamic, uniaxial tension tests. This loader has been employed by ERDC to conduct dynamic experimentation on reinforcing steel, splices, and fasteners since the 1970's [30–32], and it remains the approved validation apparatus for the dynamic testing of mechanical splices for reinforcing steel used in protective design [19].

The device was slowly pressurized by pumping compressible silicon oil into the top and bottom pressure chambers. Pressure in the top chamber was kept at a slightly higher pressure in order to maintain a small tensile preload (50-1,000 lbf) on the specimen. The measured preload ensured alignment of the specimen through the bolted connections and also seated the top reaction stem pivot joint to further ensure axial loading of the specimen. Once the desired fluid pressure was reached, a quick-opening valve leading to an empty expansion tank was opened. Pressure in the lower chamber was rapidly reduced allowing the piston to translate downward and apply a tension load to the specimen attached above. Flow rate of the fluid in the lower chamber into the expansion tank was controlled by an adjustable orifice and was the main variable in changing the loading rate (strain rate) applied to the test specimen.

The adjustable orifice allows for specimen strain rates of approximately 0.001 to 4.0 s^{-1}, and the limits are dependent on specimen geometry, specimen stiffness, and oil pressure. The lowest strain rate recorded during experimentation was 0.002 s^{-1} with the smallest obtainable orifice setting, and the highest was 2.91 s^{-1} with the largest orifice setting. The UFC lists strain rates for bending, tension, and compression modes at various pressure levels. Provided strain rates range from 0.02 to 0.30 s^{-1} [19], and were well within the strain rate limits of the hydraulic loader.
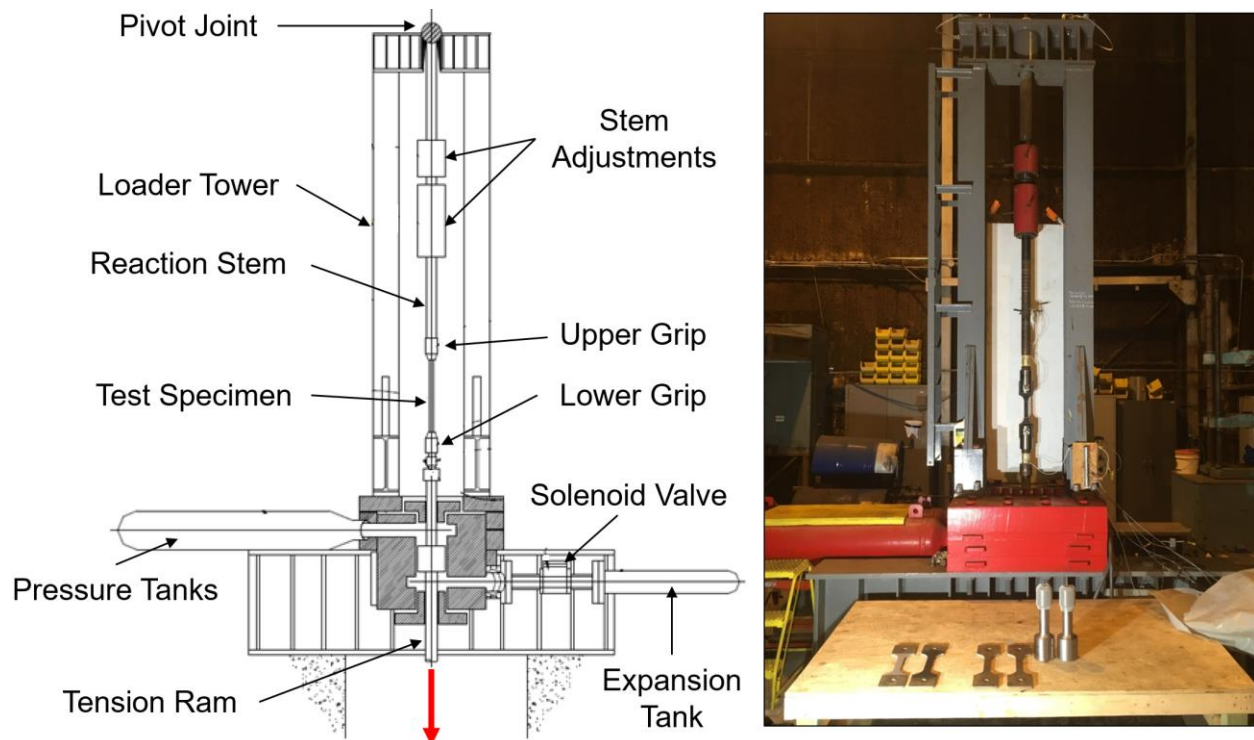
Figure 4. ERDC's 200-kip-capacity hydraulic dynamic loading machine.

Instrumentation

Strain

Axial deformation was measured using a Phantom Miro 320S high-speed (HS) camera. The HS camera recorded locations of gauge marks from time zero (trigger) through fracture of the specimen. The video was uploaded into Image System's TrackEye Motion Analysis (TEMA) software [33], which incorporated an optical extensometer feature that tracked each gauge mark location, represented by a single pixel, frame by frame throughout the length of the video recording. The software then output the distance between gauge marks (elongation) with respect to time as they moved from pixel to pixel. Quadrant markers were added to the specimen to enhance the tracking capabilities of the TEMA software. Pixel length was determined by the vertical resolution of the HS camera recording and the distance between the tracked points. The vertical resolution was set to the maximum of 1,200 pixels, which provided an elongation measurement accurate to approximately 0.00105 in., or 185 microns of strain, for the rates of 0.002 to 0.05 s^{-1}. At higher strain rates, the collection rate was increased, forcing the vertical resolution to be reduced to 904 pixels, which allowed an approximate accuracy of 0.00155 in. for elongation and 255 microns for strain. The HS camera software was calibrated to remove error due to lens distortion using the prescribed TEMA lens calibration guidelines [33].

Even with a collection rate of 13,000 frames per second, for experiments conducted at the highest rate (≈ 2.0 s^{-1}) the HS camera was only able to obtain roughly 20 data points before the specimens would yield. Bonded strain gauges were implemented at this rate to obtain high resolution strain data up to yield to supplement the HS Camera data. Strain gauges were applied to specimens used for strain rate calibration and specimens tested at 2.0 s^{-1}. For these specimens, it was necessary to remove mill scale from the parent material to facilitate strain gauge bonding. Approximately 0.006 in. (< 2% of thickness) of material was removed by machining across the entire gauge region, which allowed application of a strain gauge to the exposed steel at the center of the gauge region. A schematic of the test assembly showing the dynamic specimen and locations of instrumentation is shown in Figure 5.

Load

Load was measured using two load cells in series with the 200-kip-loader tension ram. The load cells were fabricated from AISI 4130 quenched and tempered steel with a minimum yield strength of 100 ksi. The bridge network used on the load cells consisted of eight strain gauges installed in pairs at the quarter points, midway in the necked down portion of the load cell. One gauge of each pair measured axial strain and the other measured Poisson's effect. The active gauges were on the opposite sides of the bridge topology with the adjacent Poisson gauges electrically connected on opposite sides as well. Calibration of the load cells was conducted by placing both in series with a pre-calibrated, manufactured load cell. The load cells were statically calibrated to a maximum load of 200 kip. Post-test verification indicated that the load cells maintained calibration throughout all dynamic experiments.

Acceleration

Two accelerometers (Meggit, model 7280A) were used to record acceleration during experiments conducted at rates of 0.05 s^{-1} and higher. Data recorded from these devices allowed inertial load effects to be determined and removed from the load versus time history. Accelerometers were mounted in an orientation that measured positive acceleration in the upward direction.
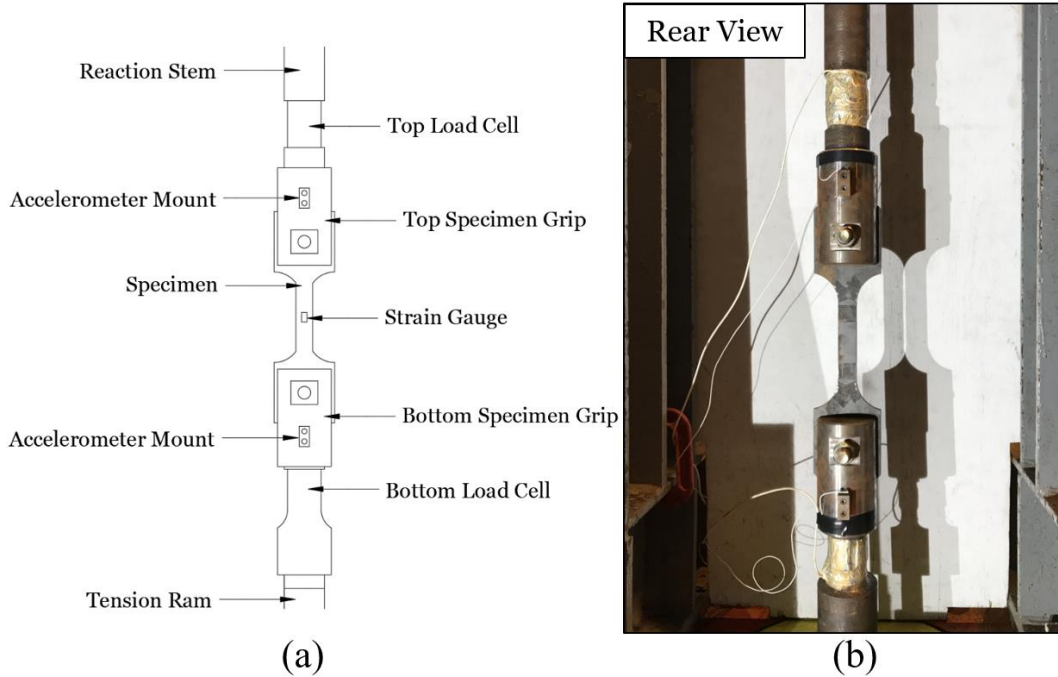

Figure 5. Schematic of test assembly (a) and dynamic specimen loaded into grips (b).

Load Analysis and Data Reduction

Inertial Force Correction

Newton's second law explains that when force is applied to objects with mass, inertial forces develop to resist the impending motion. If the objects have a large mass or if the accelerations are high, these inertial forces become quite significant. When the tension ram of the testing machine began to first apply rapid load onto the specimen through the lower grip, the mass of the grip and specimen resisted the downward acceleration. Increased load was required to overcome this inertial resistance and begin pulling the lower grip and half of the specimen downward applying tension. The lower load cell recorded, as one total load, both the applied load to the specimen and the load required to overcome inertia. Inertial force was subtracted from the bottom load cell record to form a corrected load applied to the specimen. Contrarily, addition of inertial force was required for the top load cell record to form the corrected load applied to the specimen. An uncoupled (mass) spring-mass model (Figure 6) was used to develop the required load correction equations. Equilibrium equations (Eq. 1-3) were developed to solve for the corrected load applied to the specimen.
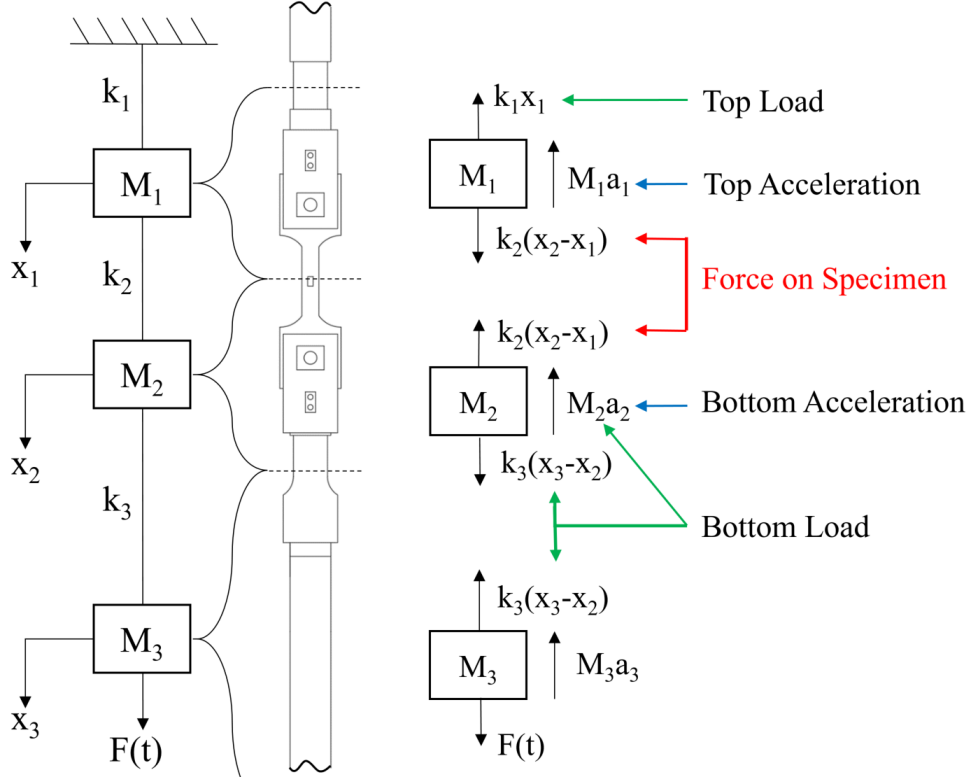
5

Figure 6. Diagram of uncoupled spring-mass model used for inertial load correction.

$$k_2(x_2 - x_1) = M_1 a_1 + k_1 x_1 \tag{1}$$

$$k_3(x_3 - x_2) = M_2 a_2 + k_2(x_2 - x_1) \tag{2}$$

$$F(t) = M_3 a_3 + k_3(x_3 - x_2) \tag{3}$$

where

$F(t)$	= applied force as function of time (lbf)
M_1	= mass of top specimen grip and half of the test specimen (lbm)
M_2	= mass of bottom specimen grip and half of test specimen (lbm)
M_3	= mass of tension ram and piston (lbm)
a_1	= acceleration of M_1 (g)
a_2	= acceleration of M_2 (g)
a_3	= acceleration of M_3 (g)
k_1	= spring constant of upper reaction member (lbf/in.)
k_2	= spring constant of test specimen (lbf/in.)
k_3	= spring constant of tension ram and piston (lbf/in.)
x_1	= displacement of M_1 (in.)
x_2	= displacement of M_2 (in.)
x_3	= displacement of M_3 (in.)

Eq. 1 represents the corrected load on the specimen using the top load cell and acceleration data. Eq. 2 was solved to determine the corrected load using the bottom load cell and acceleration data (Eq. 4).

$$k_2(x_2 - x_1) = k_3(x_3 - x_2) - M_2 a_2 \tag{4}$$

Since the accelerometers were mounted in an orientation that recorded positive acceleration in the upward direction, accelerations in Eq. 1 and Eq. 4 were corrected by switching the signs of a_1 and a_2 to form Eq. 5 and Eq. 6, respectively. Substitution allows for Eq. 7 to be derived, which states that the corrected load using the top data records, load and acceleration, should theoretically be equal to the corrected load using the bottom data records. Testing at the static rate (0.00002 s⁻¹) and the dynamic rate of 0.002 s⁻¹ produced accelerations of insignificant magnitudes and were therefore neglected.

$$k_2(x_2 - x_1) = k_1 x_1 - M_1 a_1 \tag{5}$$

$$k_2(x_2 - x_1) = k_3(x_3 - x_2) + M_2 a_2 \tag{6}$$

$$k_1 x_1 - M_1 a_1 = k_3(x_3 - x_2) + M_2 a_2 \tag{7}$$

Figures 7-8a shows an example inertial force correction for both the top and bottom load cell data for the highest strain rate experiments (≈ 2.0 s⁻¹). The bottom load cell, attached to the tension ram of the loader, experiences up to four times the acceleration of the upper; therefore, the inertial load correction is much more significant on the bottom load cell data. The average of the corrected top and corrected bottom load versus time histories are used for the calculation of engineering stress.
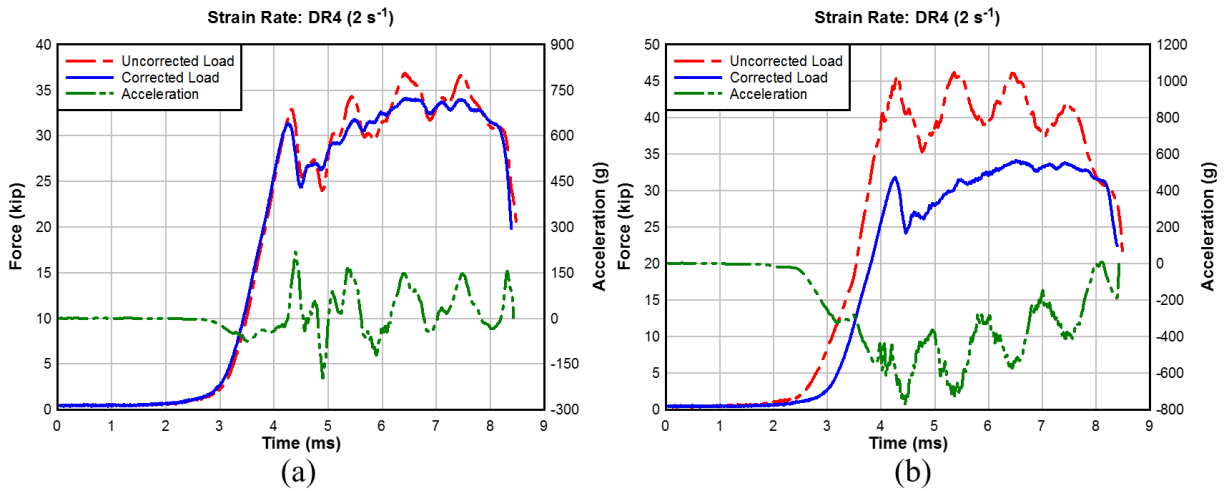

Figure 7. Top (a) and bottom (b) inertial load correction using acceleration data.
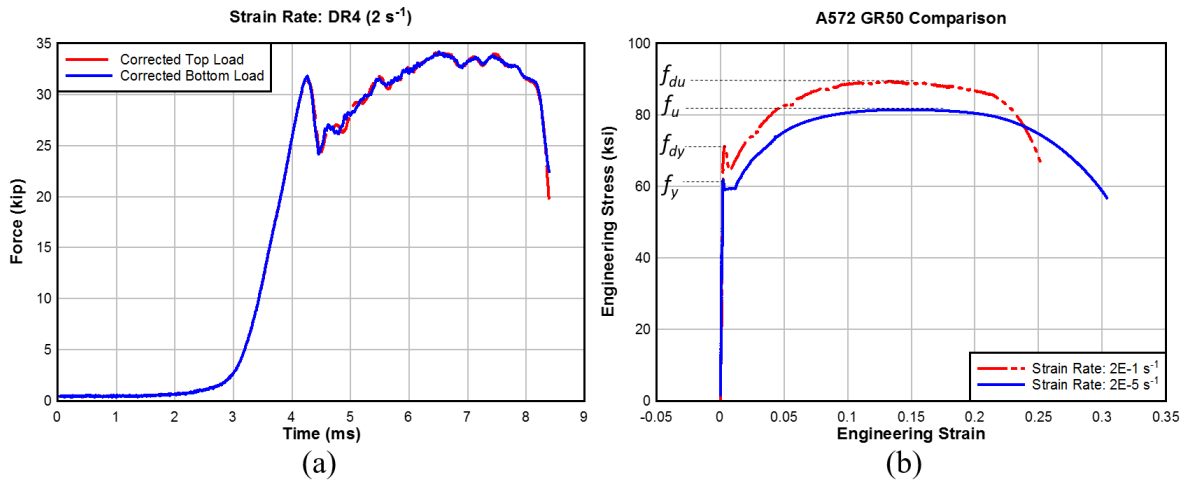

Figure 8: Corrected load comparison (a). Static and dynamic stress-strain diagram of A572-50, identifying terms of Eq. 8-9 (b).

7

Data Analysis

The average corrected load was divided by the original cross section of the test specimen to calculate engineering stress. Average strain was determined from elongation data. Stress was plotted as a function of strain to develop the stress-strain diagram for each test. Upper yield strength was determined as the stress corresponding to the maximum force at the onset of discontinuous yielding as prescribed in ASTM E8-7.7.3 [29]. Ultimate tensile strength was calculated by dividing the maximum force applied to the specimen during the test by the original cross-sectional area of the specimen (E8-7.10 [29]). The strength properties were rounded to the nearest 0.1 ksi. Strain rate was determined by calculating the slope of the strain-time data in the elastic deformation region.

The ratio of dynamic-to-static yield stress is defined as the dynamic increase factor (DIF_y) at a specified strain rate. The tested A572-50 and A992 steels both exhibited discontinuous yielding. ASTM specifies minimum yield stress values for these steels based on the yield point [29]; therefore, the yield point (upper yield strength) was used in determining DIF_y using Eq. 8. Figure 8b indicates the values used in the equations below on a static and dynamic stress-strain diagram.

$$DIF_y = \frac{f_{dy}}{f_y} \qquad (8)$$

$$DIF_u = \frac{f_{du}}{f_u} \qquad (9)$$

where

DIF_y	= dynamic increase factor for yield strength for a particular strain-rate
DIF_u	= dynamic increase factor for ultimate tensile strength for a particular strain rate
f_{dy}	= dynamic yield strength at a particular strain rate above static (ksi)
f_{du}	= dynamic ultimate tensile strength at a particular strain rate above static (ksi)
f_y	= average yield strength measured during static testing (ksi)
f_u	= average ultimate tensile strength measured during static testing (ksi)

RESULTS

Eight static-rate tension tests were originally conducted for each steel. Six more were required to verify the static properties of a surplus A992 beam that was obtained to fabricate additional specimens required to complete the dynamic experiments. A minimum of five dynamic-rate tension tests were conducted at each rate. In some cases additional dynamic tests were conducted to compensate for specimens that fractured on gauge marks. A comparison of load histories between specimens that fractured on gauge marks and those that did not indicated no identifiable impact on yield strength or UTS; therefore, results from these experiments were included in the analysis of DIF data. Ductility properties for the specimen that fractured on gauge marks were uncharacteristically low and were not included in percent elongation or reduction of area analysis.

Table 2 lists the number of tension tests conducted at each target strain rate. The average material strength values and standard deviations for each target strain rate are listed in Tables 3-4. The strain rate corresponding to each targeted rate could not be kept constant between tests; however, dynamic yield and UTS values were obtained without a substantial amount of distribution when grouped by target strain rate. Standard deviation for the static yield strength was 0.27 ksi for A572-50 and 1.38 ksi for A992. The static UTS standard deviation was 1.43 ksi for A572-50 and 0.48 ksi for A992. Deviations for the dynamic-rate tests were of a similar order of magnitude as the static.

Table 2. Uniaxial tension test matrix.

Material	Target Strain Rate (s⁻¹)	# Tests
A572-50	0.00002 (Static)	8
	0.002 (DR1)	5
	0.05 (DR2)	8
	0.2 (DR3)	5
	2.0 (DR4)	6
	Total	32
A992	0.00002 (Static)	14
	0.002 (DR1)	5
	0.05 (DR2)	7
	0.2 (DR3)	5
	2.0 (DR4)	10
	Total	41

Table 3. Average material strength properties of A572-50 at increasing strain rates.

Target Strain Rate (s⁻¹)	Standard Deviation Strain rate (s⁻¹)	Average Yield Strength (ksi)	Standard Deviation Yield Strength (ksi)	Average UTS (ksi)	Standard Deviation UTS (ksi)
0.00002 (Static)	2.3E-06	61.5	0.27	81.9	1.43
0.002 (DR1)	9.4E-05	65.7	1.37	85.4	0.36
0.05 (DR2)	5.9E-03	69.8	1.20	87.5	0.42
0.2 (DR3)	2.1E-02	71.7	1.24	89.8	0.55
2.0 (DR4)	1.8E-01	83.5	0.85	97.9	0.90

Table 4. Average material strength properties of A992 at increasing strain rates.

Target Strain Rate (s⁻¹)	Standard Deviation Strain rate (s⁻¹)	Average Yield Strength (ksi)	Standard Deviation Yield Strength (ksi)	Average UTS (ksi)	Standard Deviation UTS (ksi)
0.00002 (Static)	2.3E-06	54.0	1.38	68.9	0.48
0.002 (DR1)	9.4E-05	60.3	1.13	71.6	0.53
0.05 (DR2)	5.9E-03	64.3	1.20	73.9	0.27
0.2 (DR3)	2.1E-02	67.6	0.70	76.2	0.18
2.0 (DR4)	1.8E-01	78.1	1.00	83.4	0.39

The measured yield strength and UTS for each experiment are shown in Figure 9. Static yield strength (f_y) and UTS (f_u) were determined by averaging values obtained from static testing of each material. The DIF for yield (DIF_y) and UTS (DIF_u) were calculated with Eq. 8 and Eq. 9, respectively. The calculated values were graphed in DPlot software [34]. Analysis of the data led to formulation of a bi-linear least-squares regression curve fit on a log-linear DIF versus strain rate plot. Individual values for each experiment and curve fits are shown in Figure 10. The percent elongation after fracture and percent reduction of area for each experiment are shown in Figure 11a.
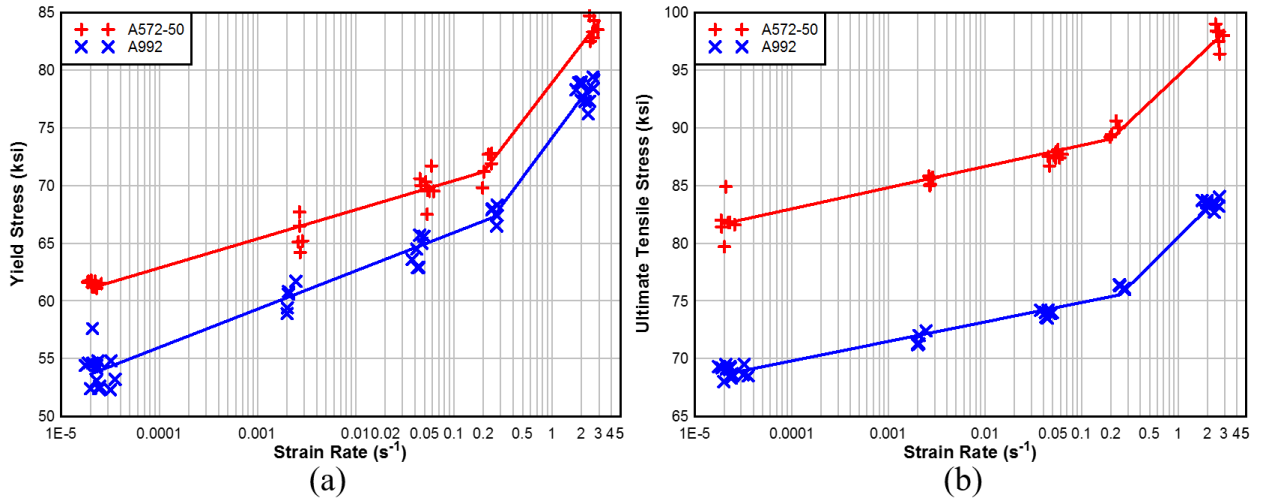
Figure 9. Measured yield strength (a) and UTS (b) of A572-50 and A992 steel at increasing strain rates.
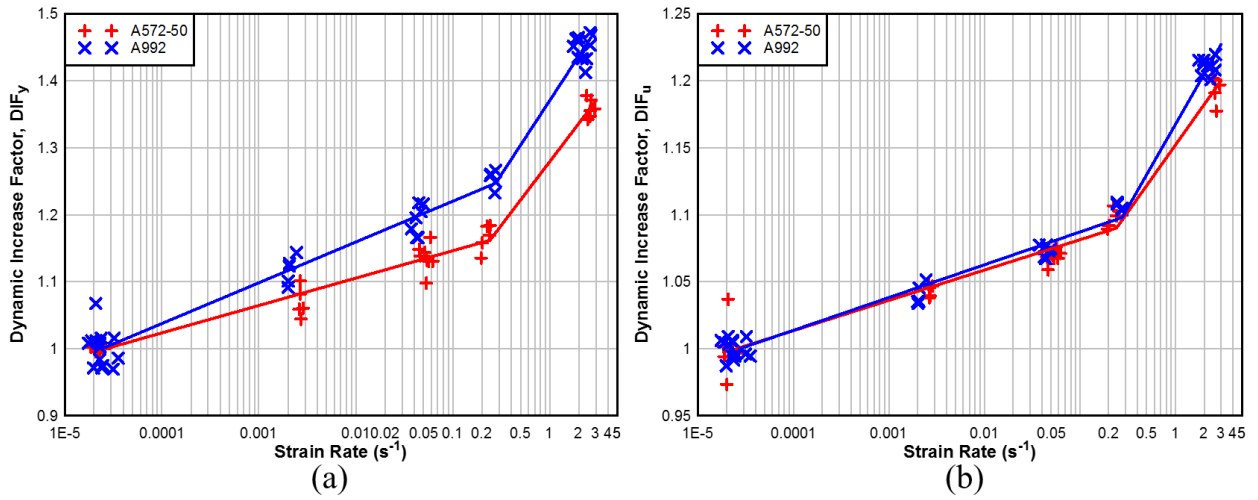

Figure 10. Experimental dynamic increase factors of yield (a) and UTS (b) for A572-50 and A992 steel.
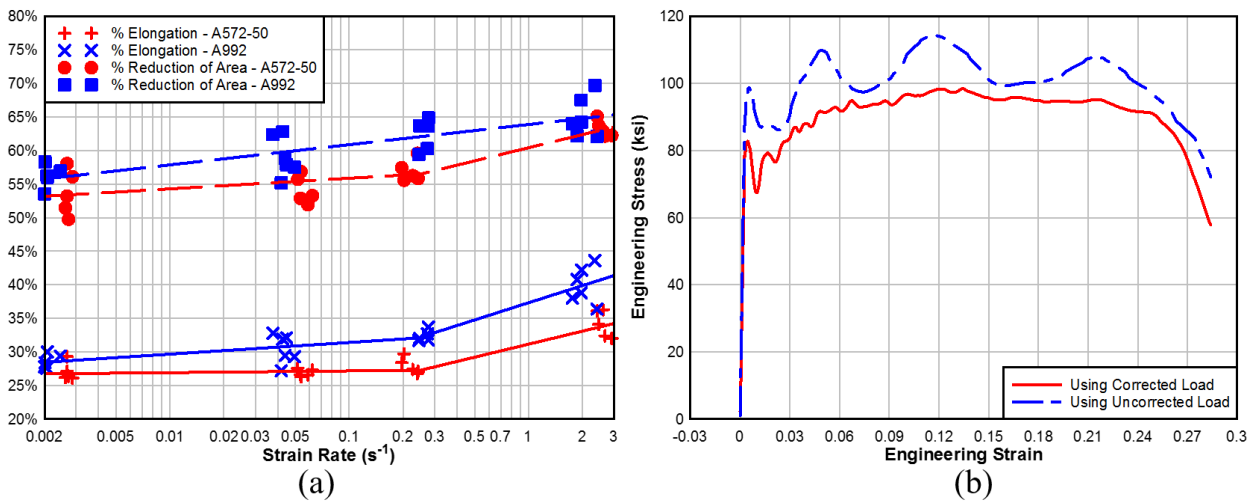

Figure 11. Measured ductility properties of A572-50 and A992 steel at increasing strain rates (a). Stress-strain diagram with and without inertial load correction at a strain rate of 2.0 s⁻¹ (b).

DISCUSSION

Influence of load correction on the stress-strain curves at 2.0 s^{-1} is shown in Figure 11b. The illustration indicates how the determination of experimental material strength properties can be substantially impacted if inertial forces are neglected during higher strain rate tension tests. The amount of inertial load correction required increased as test component mass and acceleration increased.

The DR4 stress-strain curves for both steels exhibited oscillations after yielding despite inertial load corrections, which can be partially attributed to stress wave propagation through the loading ram and specimen after yield. Wave propagation speed, which is neglected in these experiments, plays an increased role in recording material response as strain rate increases. There is a slight difference in time between the instantaneous response of the material in the gauge region of the specimen and the measured response captured by the load cells and accelerometers located a finite distance away from the gauge region. The small difference in time domains contributes to the un-smooth stress-strain curves for the DR4 experiments. Impacts of this phenomena on upper yield strength and UTS at DR4 are negligible; however, the lower yield strength and yield plateau regions of the stress-strain diagrams can be greatly masked by this effect. If DIF data were desired for strain rates greater than tested during this research (>10 s^{-1}), stress wave propagation factors would likely have a much greater influence on the material response and must be factored into the measured material properties.

The experimental data for both DIF_y and DIF_u exhibited a bi-linear trend with a transition in slope between the rates of 0.2 and 2.0 s^{-1}. Change in strain rate sensitivity, represented by change in slope of the DIF curves, has been documented for many materials [2,35–39] and is associated with different "regions" of strain rate sensitivity that are dependent on temperature. Figure 12a [39] depicts an example of yield strength sensitivity regions with respect to strain rate and temperature for steels. An additional example indicating drastic changes in strain rate sensitivity is also shown in Figure 12b [36], which was compiled by Hong and Kang from experimental data regarding tensile properties of concrete. Shaded boxes added by the authors of this report roughly separate different regions of strain rate sensitivity for that material. Acquisition of additional DIF data between DR3, DR4, and beyond would provide more information on the strain rate sensitivity in the transformation region of A572-50 and A992 steels.
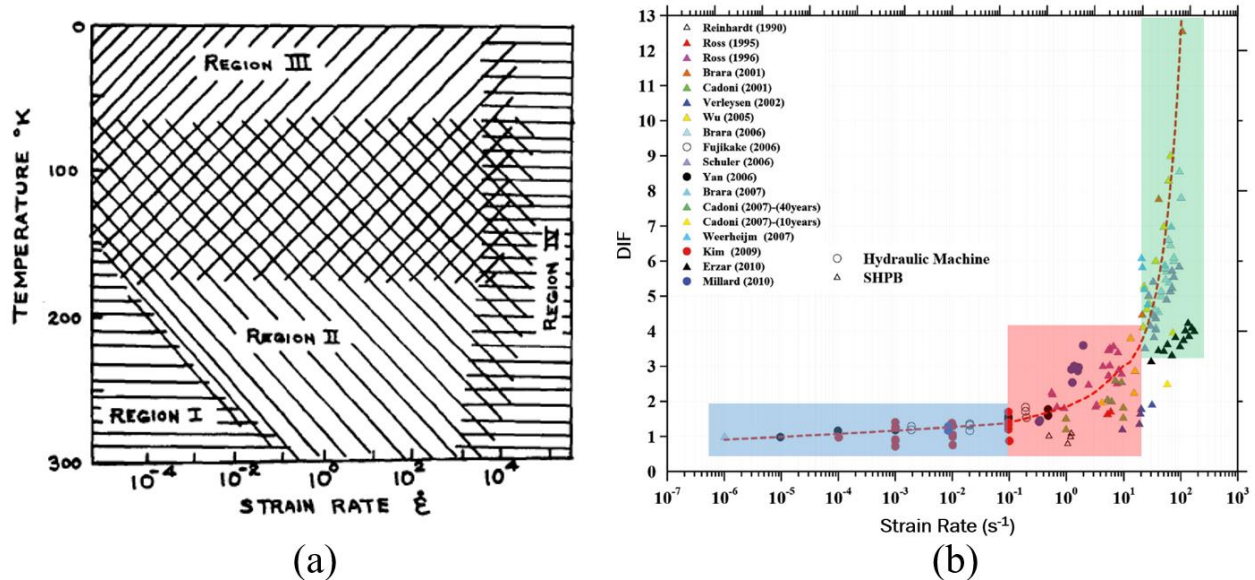

(a)   (b)

Figure 12. General regions for yield strength sensitivity of steel to strain rate and temperature [39] (a). Strain rate effect on tensile strength of concrete (adapted from [36]) (b).

The static yield strength of the A572-50 (61.5 ksi) was substantially greater than that of the A992 (54 ksi), even though both steels have a specified minimum yield of 50 ksi. The difference in static yield strength likely explains why A992 displayed higher strain rate sensitivity, as previous research has shown an inverse relation between DIF_y and static yield strength [22,36]. Malvar [22] documented how DIF_y values for reinforcing steel are highly related to static yield

strength values and established an empirical formula to approximate DIF_y values of various grades of reinforcing steel based on static yield strength values alone. DIF_y results for the structural steels were compared to Malvar's approximation formula for reinforcing steel in Figure 13a. Differences between the experimental results and Malvar's approximation equation can most likely be attributed to the difference in chemical composition between structural and reinforcing steels.
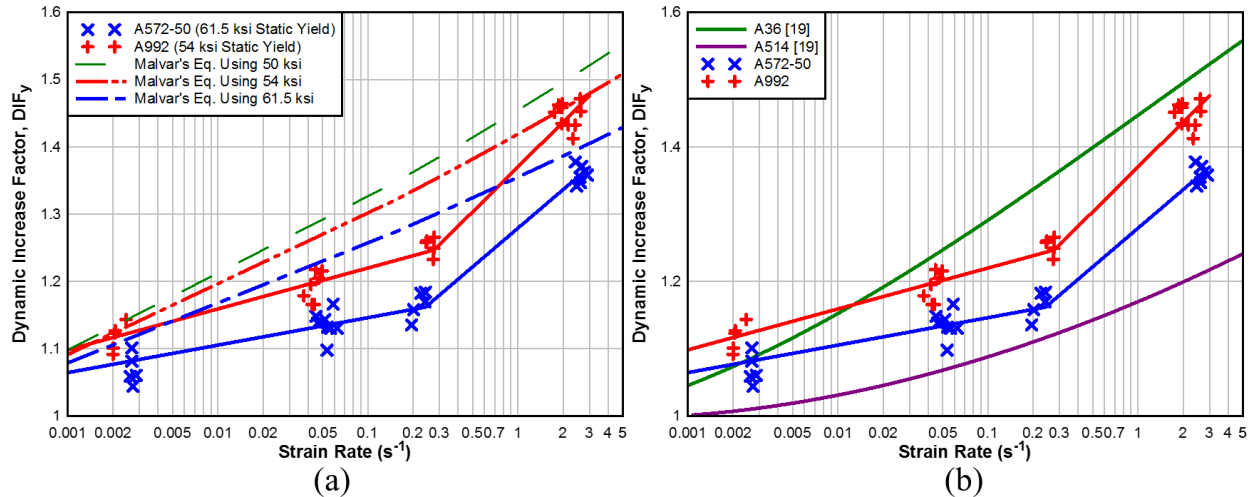

Figure 13. Comparison of experimental DIF_y data of structural steel and Malvar's approximation formula [22] for reinforcing steel (a). Comparison of experimental results to UFC [19] values of A36 and A514 (b).

The DIF_y curves developed from the experimental data were added to Figure 5-2 of the UFC [19] and shown in Figure 13b. It is uncertain how the A36 and A514 design curves were formulated, as the source of data for these steels remains unavailable. It would be logical for the curves of A992 and A572-50 to lay between those of A36 and A514 because of the difference in static yield strength values. Without the report(s) that detail the A36 data, it is difficult to determine why the DIF_y values for A992 and A572-50 measured above A36 for strain rates under 0.02 s^{-1}.

In 1969, Cowell conducted dynamic experiments on many different structural steels; A36, A441, Ex-Ten 50, and A242 [40]. Cowell indicated that Ex-Ten 50 was a columbium-vanadium steel representative of A572-50. The average static yield strength for the Ex-Ten that was tested measured 56 ksi. The DIF_y values were much higher for Ex-Ten 50 than what was measured for A572-50, but compared well when the lower yield strength was used to determine the DIF_y for the Ex-Ten (Figure 14a).
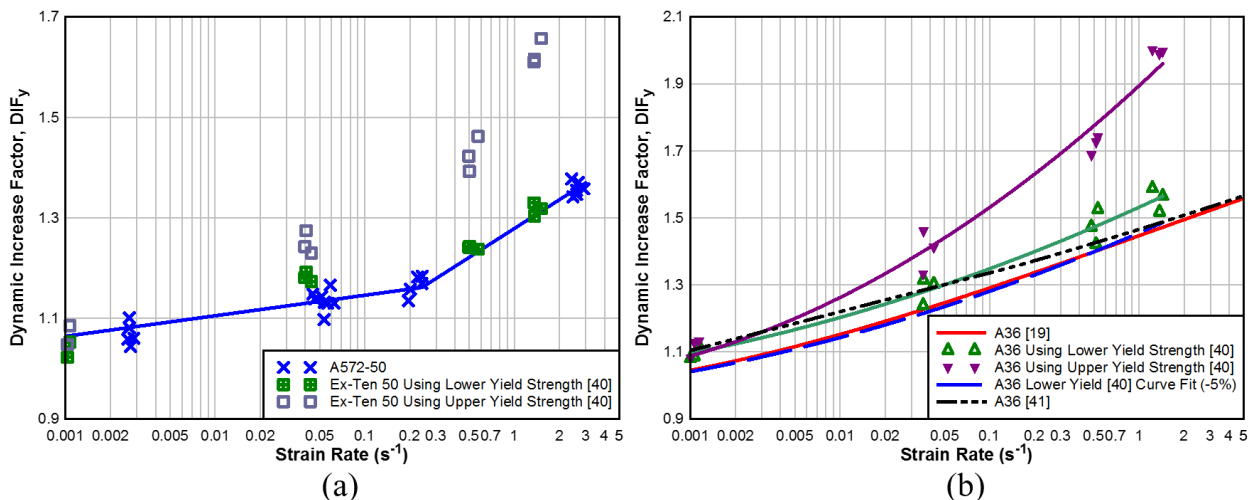

Figure 14. Comparison of A572 experimental results and Cowell's Ex-Ten 50 [40] (a). Comparison of DIF_y values of A36 steel from Cowell [40], Lucon [41], and the UFC [19] (b).

12

Figure 14b compares the A36 DIF_y values obtained by Cowell [40] and the current UFC [19] DIF_y values. A curve fit from additional high-rate testing of A36 steel conducted by Lucon [41] was also added for comparison. It is unknown why Cowell used the lower yield strength values to calculate the DIF_y during this research; however, it is clear that the values obtained using Cowell's testing machine and instrumentation seem much higher than would be expected. It is interesting, however, to note how closely the UFC A36 DIF design curve follows the least-squares curve fit of Cowell's A36 data. The dashed blue line in Figure 14b was generated by reducing a curve fit of Cowell's data by 5%.

Further review of Cowell's reports [40,42] and TR-331 [43], which detailed the testing machine and data collected for those experiments, indicated that acceleration was not recorded. There was also no documentation of inertial load correction, which would require acceleration data. Lack of inertial load correction would generate errors in load and stress values that increased with strain rate and is the most probable reason why Cowell's DIF_y values measured so high. A second look at Figure 11b indicates how the lower yield strength values for an uncorrected stress-strain curve could match closely to the upper yield strength value for a corrected stress-strain curve through coincidence alone. This could explain why the DIF_y values for Ex-Ten 50 in Figure 14a, calculated using lower yield strength, lay closer than those calculated using the upper yield strength when compared to the results of this research.

CONCLUSIONS

Results of an experimental program on the dynamic mechanical properties of ASTM A572-50 and A992 structural steels at elevated strain rates have been presented along with the testing techniques and procedures. Static-rate, uniaxial tension tests were conducted at a strain rate of approximately 0.00002 s^{-1}, and dynamic-rate, uniaxial tension tests were conducted at increasing strain rates of approximately 0.002, 0.05, 0.2, and 2.0 s^{-1}. Results of the experiments allowed development of experimental DIF versus strain rate curves for both yield strength and UTS of each steel.

It was determined that the load-carrying capacity for both A572-50 and A992 structural steels will increase with strain rate up to the maximum rate tested. A992 steel exhibited a slightly higher (4-7% difference) DIF for yield strength than A572-50, but less than 1% difference for UTS. A572-50 steel exhibited an increase in yield strength up to 35% and ultimate tensile strength up to 20% as strain rate increased. A992 steel exhibited a similar increase in yield strength up to 45% and ultimate tensile strength up to 20%. Strain rate sensitivity for yield strength and UTS changed for both steels with increased strain rates, which was represented by the change in slope of the DIF curves between the rates of 0.2 and 2.0 s^{-1}.

Data obtained from these experiments will be used to develop the DIF design curves for addition into chapter five of UFC 3-340-02, and will allow engineers to efficiently design structural steel members to resist dynamic loadings. Both steels tested during these experiments were produced domestically. It is highly recommended that additional testing on foreign-produced A572-50 and A992 specified steels be conducted to ensure the strain rate sensitivities match those of domestic.

ACKNOWLEDGMENTS

REFERENCES

1. Eleiche, A.-S. "A Literature Survey of the Combined Effects of Strain Rate and Elevated Temperature on the Mechanical Properties of Metals." Technical Report AFML-TR-72-125. Wright-Patterson Air Force Base, OH: Air Force Materials Laboratory: Air Force Systems Command, September 1972.
2. Lindholm, U. "A Survey of Rate Dependent Strength Properties of Metals." Technical Report AFML-TR-69-119. Wright-Patterson Air Force Base, OH: Air Force Materials Laboratory: Air Force Systems Command, April 1969.

3. Samanta, S. "Resistance to Dynamic Compression of Low-Carbon Steel and Alloy Steels at Elevated Temperatures and at High Strain-Rates." *International Journal of Mechanical Sciences* 10, no. 8 (August 1, 1968): 613–36.

4. Soroushian, P., and K.-B. Choi. "Steel Mechanical Properties at Different Strain Rates." *Journal of Structural Engineering* 113, no. 4 (April 1987): 663–72.

5. Elam, C. F. "The Influence of Rate of Deformation on the Tensile Test with Special Reference to the Yield Point in Iron and Steel." *Proceedings of the Royal Society of London. Series A. Mathematical and Physical Sciences* 165, no. 923 (April 27, 1938): 568–92.

6. Eleiche, A. M., and J. D. Campbell. "The Influence of Strain-Rate History and Temperature on the Shear Strength of Copper, Titanium and Mild Steel." Technical Report AFML-TR-76-90. Wright-Patterson Air Force Base, OH: Air Force Materials Laboratory, March 1976.

7. Work, C. E., and T. J. Dolan. "The Influence of Temperature and Rate of Strain on the Properties of Metals in Torsion." Technical Report WADC TR 53-10. University of Illinois, February 1953.

8. Asay, J.R., and G.I. Kerley. "The Response of Materials to Dynamic Loading." *International Journal of Impact Engineering* 5, no. 1–4 (January 1987): 69–99.

9. Yongning, L., Z. Jinhua, Z. Huijiu, and P. S. Follansbee. "Variation of Yield Stress with Strain Rate for Three Carbon Steels." *Journal of Engineering Materials and Technology* 114, no. 4 (1992): 348.

10. Inhaber, H. "Variation of Yield Stress with Strain and Strain Rate in Mild Steel." *Journal of Engineering for Industry* 89, no. 3 (August 1, 1967): 478–81.

11. El-Magd, E. "Mechanical Properties at High Strain Rates." *Le Journal de Physique IV* 04, no. C8 (September 1994): C8-149-C8-170.

12. Kendall, D. P. "The Effect of Strain Rate and Temperature on Yielding in Steels." *Journal of Basic Engineering* 94, no. 1 (March 1, 1972): 207–12.

13. Kendall, D. P., and T. E. Davidson. "The Effect of Strain Rate on Yielding in High Strength Steels." *Journal of Basic Engineering* 88, no. 1 (March 1, 1966): 37–44.

14. Maiden, C. J., and S. J. Green. "Compressive Strain-Rate Tests on Six Selected Materials at Strain Rates from 10^{-3} to 10^4 In/In/Sec." *Journal of Applied Mechanics* 33, no. 3 (September 1, 1966): 496–504.

15. Moon, D. P., and J. E. Campbell. "Effects of Moderately High Strain Rates on the Tensile Properties of Metals." DMIC-MEMO-142. Columbus, OH: Defense Metals Information Center, Battelle Memorial Institute, December 1961.

16. Rao, N., M. Lohrmann, and L. Tall. "Effect of Strain Rate on the Yield Stress of Structural Steels." *Journal of Materials* 1, no. 1 (1966).

17. Stout, M. G., and P. S. Follansbee. "Strain Rate Sensitivity, Strain Hardening, and Yield Behavior of 304L Stainless Steel." *Journal of Engineering Materials and Technology* 108, no. 4 (October 1, 1986): 344–53.

18. Singh, M., D. Sood, R. K. Gupta, R. Kumar, P. C. Gautam, B. Sewak, A. C. Sharma, and T. Mathew. "Dynamic Yield Strength of Mild Steel under Impact Loading." *Defense Science Journal* 58 (March 31, 2008).

19. Department of Defense. *Structures to Resist the Effects of Accidental Explosions*. Change 2. UFC 3-340–02. Department of Defense, 2014.

20. Healey, J., A. Ammar, J. Vellozzi, G. Pecone, S. Weissman, and N. Dobbs. "Design of Steel Structures to Resist the Effects of HE Explosions." Technical Report 4837. Dover, NJ: Picatinny Arsenal, 1975.

21. U.S. Army Corps of Engineers. *Design of Structures to Resist the Effects of Atomic Weapons*. Engineering Manual EM 1110-345-414. Strength of Materials and Structural Elements, March 1957.

22. Malvar, L. J. "Review of Static and Dynamic Properties of Steel Reinforcing Bars." *Materials Journal* 95, no. 5 (September 1, 1998): 609–16.

23. Malvar, L. J., and J. E. Crawford. "Dynamic Increase Factors for Steel Reinforcing Bars." Port Hueneme, CA: Naval Facilities Engineering Service Center, August 1998.

24. ASTM International. *ASTM A572/A572M-18 Standard Specification for High-Strength Low-Alloy Columbium-Vanadium Structural Steel*. West Conshohocken, PA; ASTM International, 2018.

25. ASTM International. *ASTM A709/A709M-17e1 Standard Specification for Structural Steel for Bridges*. West Conshohocken, PA; ASTM International, 2017.

26. ASTM International. *ASTM A992/A992M-11(2015) Standard Specification for Structural Steel Shapes*. West Conshohocken, PA; ASTM International, 2015.

27. ASTM International. *ASTM A6/A6M-17a Standard Specification for General Requirements for Rolled Structural Steel Bars, Plates, Shapes, and Sheet Piling*. West Conshohocken, PA; ASTM International, 2017.
28. ASTM International. *ASTM A36/A36M-14 Standard Specification for Carbon Structural Steel*. West Conshohocken, PA; ASTM International, 2014.
29. ASTM International. *ASTM E8/E8M-16a Standard Test Methods for Tension Testing of Metallic Materials*. West Conshohocken, PA; ASTM International, 2016.
30. Rowell, S. P., C. E. Grey, S. C. Woodson, and K. P. Hager. "High Strain-Rate Testing of Mechanical Couplers." Technical Report TR-09-8. Vicksburg, MS: U.S. Army Engineer Research and Development Center, September 2009.
31. Weathersby, J. "Investigation of Bond Slip between Concrete and Steel Reinforcement under Dynamic Loading Conditions." Technical Report TR-03-9. Vicksburg, MS: U.S. Army Engineer Research and Development Center, 2003.
32. Rabalais, C. P. "Analysis of Bolt and Rivet Structural Fasteners Subjected to Dynamic and Quasi-Static Shear Loadings." Civil Engineering Thesis, Texas A&M University, 2015.
33. Image Systems AB. "TrackEye Motion Analysis (TEMA) User's Guide." Image Systems AB, 2015.
34. Hyde, D. *DPlot* (version 2.3.5.4). Vicksburg, MS: HydeSoft Computing, 2018.
35. Flathau, W. H. "Dynamic Tests of Large Reinforcing Bar Splices." Technical Report N-71-2. Vicksburg, MS: U.S. Army Engineer Waterways Experiment Station, April 1971.
36. Hong, S., and T. H.-K. Kang. "Dynamic Strength Properties of Concrete and Reinforcing Steel Subject to Extreme Loads." *ACI Structural Journal* 113, no. 5 (September 2016).
37. Manjoine, M. "Influence of Rate of Strain and Temperature on Yield Stresses of Mild Steel." *Journal of Applied Mechanics* 11 (1944): 211–18.
38. Moćko, W., and L. Kruszka. "Results of Strain Rate and Temperature on Mechanical Properties of Selected Structural Steels." *Procedia Engineering*, Modern Building Materials, Structures and Techniques, 57 (January 1, 2013): 789–97.
39. Soohoo, P. C., C. Jiang, and M. Chen. "Dynamic Properties of Steels." Technical Report AMMRC CTR 74-24. Watertown, MA: Army Materials and Mechanics Research Center, 1974.
40. Cowell, W. L. "Dynamic Tests on Selected Structural Steels." Technical Report R-642. Port Hueneme, CA: U.S. Naval Civil Engineering Laboratory, September 1, 1969.
41. Lucon, E. "Experimental Assessment of the Equivalent Strain Rate for an Instrumented Charpy Test." *Journal of Research of the National Institute of Standards and Technology* 121 (April 2016): 165.
42. Cowell, W. L. "Dynamic Tests on High Strength Steel." Technical Note N-427. Port Hueneme, CA: U.S. Naval Civil Engineering Laboratory, February 1962.
42. Cowell, W. L. "NCEL Dynamic Testing Machine." Technical Report R-331. Port Hueneme, CA: U.S. Naval Civil Engineering Laboratory, October 30, 1964.